JACS
JOURNAL OF THE AMERICAN CHEMICAL SOCIETY

Article

pubs.acs.org/JACS

Ultralow-Power Near Infrared Lamp Light Operable Targeted Organic Nanoparticle Photodynamic Therapy

Ling Huang,[†,‡] Zhanjun Li,[†] Yang Zhao,[†,§] Yuanwei Zhang,[†] Shuang Wu,[‡] Jianzhang Zhao,[‡] and Gang Han*[,†]

[†]Department of Biochemistry and Molecular Pharmacology, University of Massachusetts Medical School, Worcester, Massachusetts 01605, United States

[‡]State Key Laboratory of Fine Chemicals, School of Chemical Engineering, Dalian University of Technology, E-208 West Campus, 2 Ling-Gong Road, Dalian 116024, P. R. China

[§]Department of Radiology, The Second Hospital of Tianjin Medical University, Tianjin, 300211 China

Supporting Information

ABSTRACT: Tissue penetration depth is a major challenge in practical photodynamic therapy (PDT). A biocompatible and highly effective near infrared (NIR)-light-absorbing carbazole-substituted BODIPY (**Car-BDP**) molecule is reported as a class of imaging-guidable deep-tissue activatable photosensitizers for PDT. **Car-BDP** possesses an intense, broad NIR absorption band (600−800 nm) with a remarkably high singlet oxygen quantum yield (Φ_Δ = 67%). After being encapsulated with biodegradable PLA−PEG-FA polymers, **Car-BDP** can form uniform and small organic nanoparticles that are water-soluble and tumor-targetable. Rather than using laser light, such nanoparticles offer an unprecedented deep-tissue, tumor targeting photodynamic therapeutic effect by using an exceptionally low-power-density and cost-effective lamp light (12 mW cm^{-2}). In addition, these nanoparticles can be simultaneously traced in vivo due to their excellent NIR fluorescence. This study signals a major step forward in photodynamic therapy by developing a new class of NIR-absorbing biocompatible organic nanoparticles for effective targeting and treatment of deep-tissue tumors. This work also provides a potential new platform for precise tumor-targeting theranostics and novel opportunities for future affordable clinical cancer treatment.

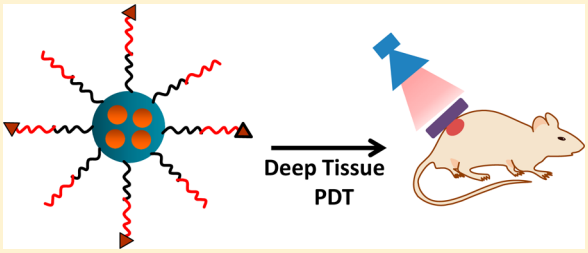

INTRODUCTION

Photodynamic therapy (PDT) is a rapidly developing cancer treatment due to its minimally invasive nature, fewer side effects, and less damage to marginal tissues than occur with conventional cancer treatments such as chemotherapy and radiotherapy.[1] In the past two decades, PDT has attracted increasing attention both in fundamental research and clinical practice.[2−4] Generally, PDT utilizes a photosensitizer that works as a light-sensitive drug to treat the targeted tissue locally upon irradiation with light at appropriate wavelengths. The mechanism of PDT is based on the interaction between the excited photosensitizer and the surrounding molecules, which generates reactive oxygen species (ROS) such as singlet oxygen ($^1O_2$). ROS in PDT can cause oxidative damage to cancer cells and, ultimately, be used as a cancer treatment.[1−6]

Since near infrared (NIR) light has much deeper tissue penetration than visible light, considerable efforts have been made to develop NIR-light-activated PDT molecules for cancer treatment at the deep-tissue level.[7,8] However, because of their weak absorption and low singlet oxygen quantum yield upon NIR irradiation, the clinical use of PDT drugs for deep-tissue cancer treatment remains challenging; for example, the absorption of the FDA-approved PDT drug PpIX is quite weak in the NIR region.[7,8] To address this issue, lanthanide-doped up-converting nanoparticles (UCNPs) were developed as in vivo phototransducers that can be excited by NIR light and emit in the visible spectrum, overlapping with the activation wavelengths of PDT drugs.[9−11] We prepared UCNPs ($NaYF_4$:Yb,Er) conjugated with prodrug (ALA) nanocomposites for PDT of deep tumors. However, the deep tissue therapeutic outcome was suboptimal; for example, less than 60% tumor volume inhibition was observed by intratumor injection at the deep-tissue level (e.g., 6 mm) under a coherent 980 nm laser beam when compared to shallow tissue studies.[11] In addition, to date, the physiological toxicity and systemic clearance of the rare-earth components in inorganic UCNPs are unclear.[12,13]

Thus, the utilization and development of organic photosensitizer molecules that are biocompatible, biodegradable, and have intensive-absorption and high-singlet-oxygen quantum yield in the NIR region are highly desirable for deep-tissue tumor PDT.[4,5] To date, although several photosensitizers such as azo-BODIPY molecules and their loaded nanoparticles were

Received: May 25, 2016
Published: October 27, 2016

DOI: 10.1021/jacs.6b05390
J. Am. Chem. Soc. 2016, 138, 14586−14591

reported to respond to NIR light activation of such compounds, PDT typically requires a laser beam with relatively high power density (>100 mW cm^{-2}),[14−17] and such utilization was only limited to shallow-tissue PDT study.

RESULTS AND DISCUSSION

To achieve PDT in deep-tissue tumors by using only low-power-density cost-effective incoherent lamp-light excitation, we designed a carbazole-substituted BODIPY (**Car-BDP**) molecule as a new highly NIR-sensitive photosensitizer. As shown in Scheme 1, compared with currently used BODIPY photosensitizers, such as 2,6-diiodo-BODIPY (**B-1**, ε = 85 000 M^{-1} cm^{-1} at 525 nm)[18−25] and 2,6-diiodistyl-BODIPY (**B-2**, ε = 77 000 M^{-1} cm^{-1} at 630 nm; **B-3**, ε = 98 000 M^{-1} cm^{-1} at 661 nm)[26,27] (see Table S1 and Scheme S2 in the Supporting Information), BODIPY dimer[28] and BODIPY-modified iridium complexes,[29] **Car-BDP** presented significantly broader and more intense absorption in the NIR region due to the large π-core of the carbazole moiety (Figure 1a). In addition, the NIR fluorescence of **Car-BDP** had an emission peak at 755 nm, and the fluorescence quantum yield was determined (Φ_F = 4%; Figure 1b). It is worthwhile noting that such high singlet quantum yield alongside strong NIR fluorescence is rare due to the fast intersystem-crossing (ISC) rate and the consequent poor fluorescence quantum yield of most conventional used sensitizers.[30] More importantly, we found that **Car-BDP** showed a remarkably high singlet-oxygen yield (Φ_Δ = 67%).

Scheme 1. (a) Schematic Illustration of NIR-Mediated PDT; (b) Car-BDP-TNM Construction and Molecular Structures of Car-BDP, PLA−PEG, and PLA−PEG-FA

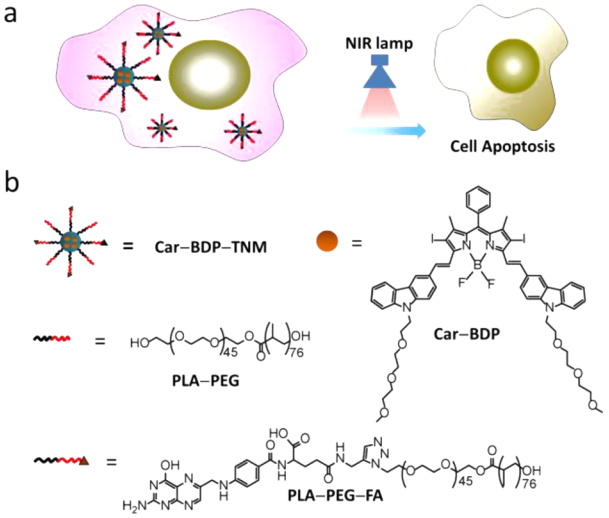

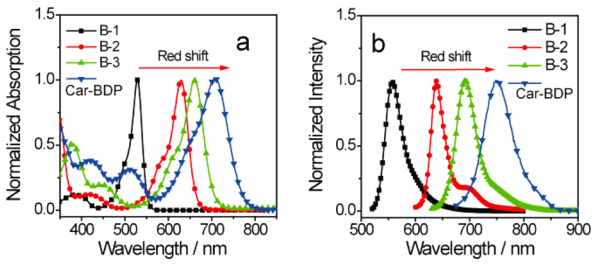

Figure 1. (a) Normalized UV−vis absorption spectra of **B-1** to **B-3** and **Car-BDP**; (b) normalized fluorescence emission spectra of **B-1** to **B-3** and **Car-BDP**.

Car-BDP molecule was water solubilized by encapsulating it with tumor targetable amphiphilic polymer PLA−PEG-FA to generate dye-loaded nanomicelles (**Car-BDP-TNM**); the dye-entrapment efficiency of **Car-BDP** in the polymer was determined to be high (74%) by the UV−vis absorption method. **Car-BDP-TNM** is significantly smaller than previously reported PDT nanoparticles.[15−17] First, the morphology and size of **Car-BDP-TNM** were measured by using transmission electron microscopy (TEM). The TEM image in Figure 2, panel b shows that **Car-BDP-TNM** consisted of uniform spherical nanoparticles with a diameter of roughly 13.7 ± 3.4 nm. In addition, the hydrodynamic diameter was 23.8 ± 3.2 nm, as measured by dynamic light scattering (DLS) experiments (Figure 2a). **Car-BDP-TNM** also showed outstanding colloidal stability in phosphate-buffered saline (PBS); after 50 days, the hydrodynamic diameter remained at 22.2 ± 2.3 nm, and no significant aggregation was observed (Figure S3).

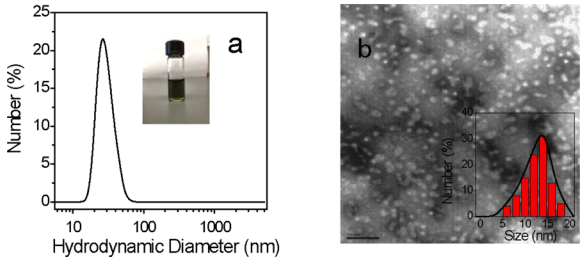

Figure 2. (a) The hydrodynamic diameter of **Car-BDP-TNM** in PBS via DLS; inset photograph shows **Car-BDP-TNM** solution. (b) TEM image of **Car-BDP-TNM** stained by phosphotungstic acid, scale bar represents 100 nm.

Next, the photophysical properties of **Car-BDP-TNM** were measured in PBS; the nanoparticles exhibited intense and broad absorption in the NIR region from 650−800 nm (Figure 3a).

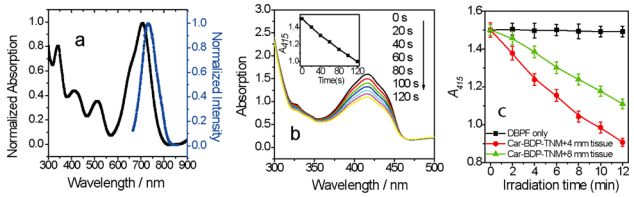

Figure 3. (a) Normalized UV−vis absorption and normalized fluorescence spectra of Car-BDP-TNM in PBS, λ_{ex} = 690 nm. (b) Change of DPBF UV−vis absorption spectra when Car-BDP-TNM was added as photosensitizer. (c) Plots of change in the optical density of DPBF at 415 nm versus the irradiation time of pork tissue of different thicknesses, where Car-BDP-TNM was used as the photosensitizer. In PBS containing 10% THF, the excitation ranged from 670−800 nm, with a power intensity of 12 mW cm^{-2} of halogen lamp light.

Car-BDP-TNM displayed NIR emission in PBS (Φ_F = 1%). This excellent NIR florescence property enables these organic nanoparticles to be simultaneously traced in vivo during the PDT. The singlet oxygen ($^1O_2$) quantum yield (Φ_Δ) induced by **Car-BDP-TNM** (Φ_Δ = 58%) under 710 nm light irradiation from an Horiba spectrometer was evaluated with 1,3-diphenylbenzofuran (DPBF) as an $^1O_2$ indicator.[31] As illustrated in Figure 3, panel b, upon addition of **Car-BDP-**

DOI: 10.1021/jacs.6b05390
J. Am. Chem. Soc. 2016, 138, 14586−14591

TNM to the solution, the absorption of the DBPF solution decreased significantly at a wavelength of 415 nm over 120 s of NIR irradiation under a ultralow-power-intensity (12 mW cm^{-2}) incoherent halogen lamp light irradiation (band-pass filter 670−800 nm), which suggests efficient generation of singlet oxygen species. Singlet oxygen generation at the deep-tissue level was also measured (Figure 3c) using varied thicknesses of pork tissue under a lamp light source. Even when the tissue was as thick as 8 mm, we still observed a significant decline in DPBF absorption. Such efficient singlet oxygen production in an aqueous solution is indeed essential for deep-tissue PDT. Moreover, **Car-BDP-TNM** exhibited superior photostability (Figure S4) and excellent pH stability (Figure S5), both of which are critical for biomedical applications.

A successful PDT photosensitizer needs to exhibit low cytotoxicity in the dark but significant cancer cell death when exposed to light. In our in vitro study, the cytotoxicity of the **Car-BDP-TNM** to HeLa cells was examined by using the MTT assay, both in the presence and the absence of irradiation with 670−800 nm light (Figure 4a). In the absence of light, **Car-BDP-TNM** was negligibly cytotoxic. In contrast, it exhibited high cytotoxicity under irradiation with the aforementioned 670−800 nm light (power intensity of 12 mW cm^{-2}). In addition, **Car-BDP-TNM** showed excellent inhibition of growth of 4T1 cells (breast cancer cells; Figures 5c and S10). Our **Car-BDP-TNM**-mediated PDT nanoparticles are superior to the widely used **ZnPc** counterpart nanoparticles (**ZnPC-NM**) with the same excitation source and power intensity (see Figure S8).

We then studied the tumor-cell-targeting ability of these nanoparticles with and without the inclusion of folate ligands.

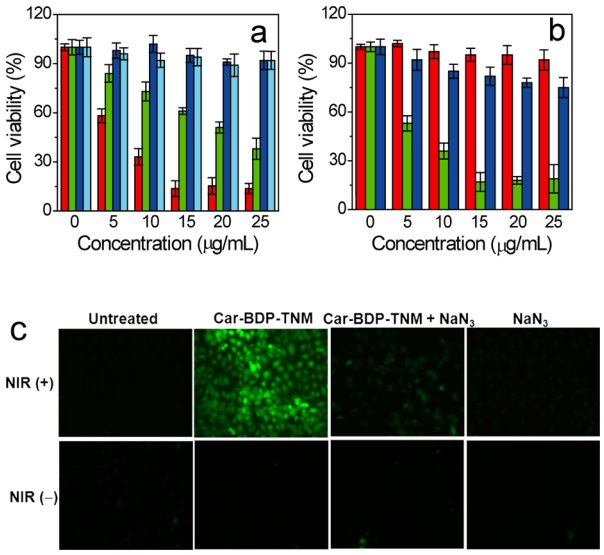

Figure 4. (a) MTT assay of HeLa cells viability of different concentrations of **Car-BDP-TNM** and **Car-BDP-NNM**: **Car-BDP-TNM** + NIR (red), **Car-BDP-NNM** + NIR (green), **Car-BDP-TNM** + dark (blue), and **Car-BDP-NNM** + dark (cyan) after treatment. (b) Sodium azide inhibition as measured by MTT assay for different concentrations of **Car-BDP-TNM** + dark (red), **Car-BDP-TNM** + NIR (green), and **Car-BDP-TNM** + NIR + NaN_3 (50 μM) (blue). (c) Fluorescence microscopy of DCFDA verified singlet-oxygen generation in **Car-BDP-TNM** (10 μg mL^{-1}); mediated intracellular λ_{ex} = 476 nm, emission detection wavelength 485−520 nm.

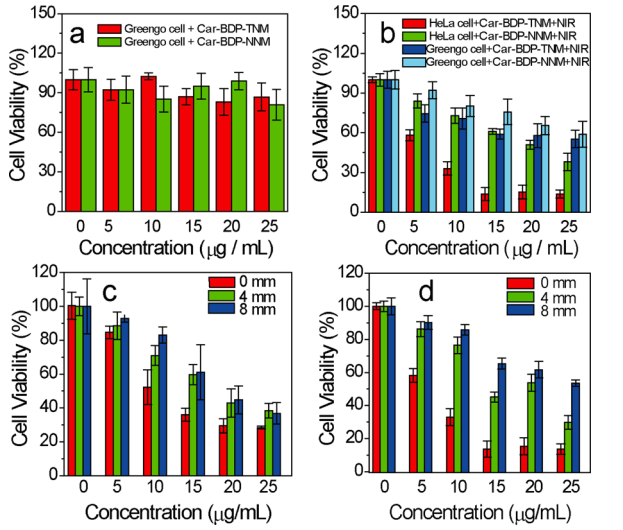

Figure 5. (a) Greengo cell viability by MTT assay in different concentrations of **Car-BDP-TNM** and **Car-BDP-NNM** in the dark; (b) compared with Greengo cells and HeLa cells viability in different concentration of **Car-BDP-TNM** and **Car-BDP-TNM** under NIR irradiation; **Car-BDP-TNM** mediated NIR deep tumor conditions in an in vitro MTT assay under different thickness tissue; (c) 4T1 cell viability. (d) HeLa cell viability. Tissue thickness was 0, 4, and 8 mm; the excitation ranged from 670−800 nm, with a power intensity of 12 mW cm^{-2} halogen lamp light.

As a control, we adopted a PLA−PEG polymer to encapsulate the Car-BDP to generate folate-free nanomicelles (**Car-BDP-NNM**) (Figure S6). In our study, HeLa cells with **Car-BDP-TNM** fluoresced more brightly than those with **Car-BDP-NNM** (Figure S12). This result shows that folate ligands indeed improve the uptake of nanoparticles. We also conducted MTT assays to evaluate **Car-BDP-TNM**- and **Car-BDP-NNM**-induced PDT effects. Figure 4, panel a shows that **Car-BDP-TNM** leads to significantly more death in cancer cells than **Car-BDP-NNM**. We also compared the phototoxicity of our system to cancer cells (i.e., HeLa) and normal cells (i.e., human skin epidermal Greengo cells). Clearly, **Car-BDP-TNM** had a higher cell-killing effect in cancers than in normal healthy tissue cell. (Figure 5b).

Further, the mechanism of **Car-BDP-TNM**-mediated PDT was validated by using fluorescence microscopy imaging with 2,7-dichlorofluorescein diacetate (DCFDA), a standard fluorescent indicator for singlet-oxygen generation in living cells.[10] Here, we observed bright green fluorescence in HeLa cells in the presence of **Car-BDP-TNM**. However, in the absence of light and sensitizer, we observed no green fluorescence. Sodium azide, a widely accepted singlet-oxygen scavenger was also used in our control experiments.[8] In the presence of sodium azide (Figure 4c), we were unable to observe green fluorescence, suggesting that sodium azide efficiently inhibited singlet-oxygen production and prevented cancer-cell death. These results clearly reveal that the generation of $^1O_2$ in **Car-BDP-TNM**-mediated PDT is in fact responsible for the death of cancer cells.

To explore whether **Car-BDP-TNM** can induce tumor cell death in a simulated deep-tissue setting, we measured **Car-BDP-TNM**-mediated PDT in different tissue thicknesses by using MTT assay. **Car-BDP-TNM** exhibited significant cell cytotoxicity at 0-, 4-, and 8-mm tissue thickness after 30 min of irradiation at 670−800 nm lamp light (power intensity of 12

DOI: 10.1021/jacs.6b05390
J. Am. Chem. Soc. 2016, 138, 14586−14591

mW cm^{-2}; Figure 5). Moreover, the fluorescence of **Car-BDP-TNM** was detectable even through an 8 mm pork tissue by using an animal imaging instrument (Figures S14 and S15). This result suggests that we are able to simultaneously image the nanoparticles in vivo while using them for therapy.

To verify the targeted tumor-killing effect of **Car-BDP-TNM** in vivo, we chose mice bearing a subcutaneous 4T1 tumor xenograft as our model. To explore the best accumulation time point of photosensitizer for PDT in the tumor tissue, the 4T1 tumor-bearing mice were intravenously injected with **Car-BDP-TNM** (50 μg mL^{-1}, 150 μL) and subjected to *in vivo* imaging at different time points (Figure 6a). As an additional control, **Car-BDP-NNM** (50 μg mL^{-1}, 150 μL) was also intravenously injected. The fluorescence at the tumor site increased gradually and reached a maximum level 24 h postinjection (Figure 6a). After 48 h, the fluorescence intensity of **Car-BDP-TNM** in the 4T1 tumor gradually decreased. However, the **Car-BDP-NNM**-treated mice display a much weaker contrast between normal and tumor tissues. This result demonstrates that folate actually improved the nanoparticle targeting to the tumor in our system.

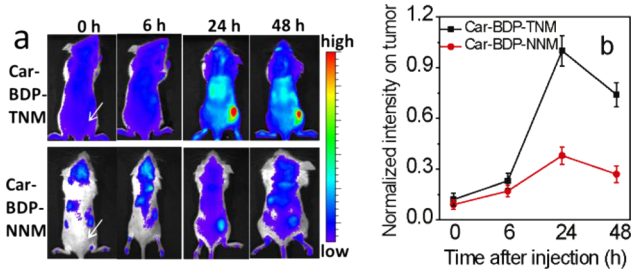

Figure 6. Specific-targeted NIR fluorescence tumor imaging in vivo. The arrows show the tumor sites. (a) Time-dependent in vivo NIR fluorescence images of 4T1 tumor-bearing mice after intravenous injection of 50 μg mL^{-1}, 150 μL, **Car-BDP-TNM** as positive group, and **Car-BDP-NNM** as negative group. (b) Normalized fluorescence intensity of **Car-BDP-TNM** and **Car-BDP-NNM** in 4T1 tumors at 6, 24, and 48 h. Data are means ± s.e.m. (n = 3 mice).

We also observed the clearance in the liver of **Car-BDP-TNM** in the same group of living tumor-bearing mice (Figure S16). Six hours after injection, a fluorescence signal started to appear in the liver. In the 6–24-h period, the fluorescence signal in the liver constantly increased. After 48 h, the fluorescence signal from the liver decreased, and after 96 h it had almost completely disappeared. This result suggests that the small size of our nanoparticles may be beneficial to the exclusion of **Car-BDP-TNM** by the liver.[32]

As the accumulation of **Car-BDP-TNM** in the tumor reached its maximum at 24 h (Figure 6a), we next examined the effect of treatment with **Car-BDP-TNM** by irradiating with lamp light (670–800 nm, 12 mW cm^{-2}) 24 h postintravenous injection. For in vivo PDT treatment, the 4T1 tumor-bearing mice were randomly divided into six groups, each group containing five mice: PBS control group (group 1), treated with light irradiation only (group 2), **Car-BDP-TNM**-intravenous-injected only (group 3), folate-free **Car-BDP-NNM**-intravenous-injected and then irradiated (group 4), **Car-BDP-TNM**-intravenous-injected and then treated with irradiation (group 5), and **Car-BDP-TNM**-intravenous-injected and then irradiated to a penetration depth of 8 mm into tissue (group 6). The PDT treatment was conducted 24 h after intravenous injection. The irradiation was performed with 670–800 nm at 12 mW cm^{-2} for 30 min (Figure 7a). After treatment, the therapeutic effects were assessed by monitoring the change in tumor volume (Figure 7b) and tumor weight (Figure 7c) as well as by hematoxylin and eosin (H&E) staining of the tumor tissues (Figure 7d). No tumor growth inhibition or tumor-tissue necrosis was observed in the group of mice with NIR only (groups 2), which indicated that irradiation with such a low power intensity NIR had little photothermal effect. In group 3, no tumor inhibition was observed, which showed that **Car-BDP-TNM** has negligible dark toxicity. Group 4 (**Car-BDP-NNM**) also did not display an obvious therapeutic effect, which suggests that folate was important for targeting tumor tissue. In contrast, the tumor growths of treatment group 5 and 6 (0 and 8 mm screening by external tissue, respectively) were remarkably suppressed. For group 5, tumor volume inhibition efficiency was found to be around 90%, and tumor-tissue weight was also significantly less (ca. 150 mg) in comparison to around 700 mg in the PBS control group (Figure 7c). From the H&E staining analysis, the tumor tissue also showed clear necrosis, which indicates that **Car-BDP-TNM** can be effectively activated by NIR lamp irradiation to be intensely phototoxic to the tumor. More importantly, in group 6, tumor volume inhibition efficiency was observed to be well preserved (ca. 80%), and tumor-tissue weight was about 210 mg, which clearly indicates that **Car-BDP-TNM** is activated in deep tissue (8 mm) and generates an effective PDT process (Figure S17). To our knowledge, this is the first time that deep-tissue setting tumor treatment was realized with such a low-power, incoherent NIR lamp irradiation.

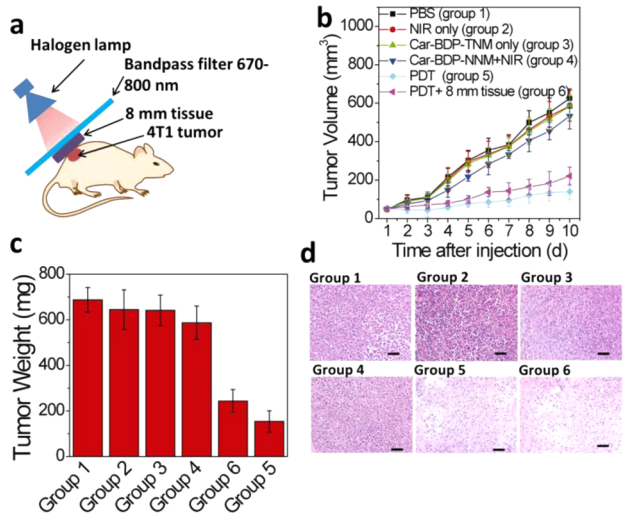

Figure 7. (a) Schematic illustration of **Car-BDP-TNM**-mediated PDT in deep tumor. (b) Tumor growth inhibition by **Car-BDP-TNM**-mediated PDT in 4T1 tumors; PDT was performed 24 h after injection of **Car-BDP-TNM** (50 μg mL^{-1}, 150 μL). Values are means ± s.e.m. (n = 5 mice per group). (c) Average weights of tumors at day 10. Mice were killed and tumors isolated for weighing. Values are means ± s.e.m. (n = 5 mice per group). (d) H&E staining of tumor-tissue sections from different treatment groups 10 days after treatment; scale bar represents 50 μm.

We evaluated the organ distribution of **Car-BDP-TNM** by using ex vivo fluorescence imaging at predetermined time intervals (24, 48, and 96 h; Figure S18). Twenty-four hours after treatment with the **Car-BDP-TNM** by intravenous injection, tumor and healthy organs including heart, liver,

DOI: 10.1021/jacs.6b05390
J. Am. Chem. Soc. 2016, 138, 14586–14591

spleen, lung, and kidney were excised from tumor-bearing mice and imaged ex vivo. An intense NIR fluorescence was seen in the excised tumor (Figure S18), which indicates efficient **Car-BDP-TNM** accumulation in the tumor and less localization in healthy organs. After 48 h, the fluorescence from the liver and the tumor reduced. By 96 h, the fluorescence of the liver and the tumor had significantly weakened. The fluorescence from the major organs matched that from the fluorescence imaging of living mice (Figure S16). We also quantified the fluorescence intensity of the tumor and each organ from the **Car-BDP-TNM**-treated group at different time periods. The fluorescence intensity of the tumor was higher than that in healthy organs except the liver at 24 h (Figure S18d). However, after 48 h, the fluorescence from the liver was reduced by half, but that from the tumor only reduced by 10%. At 96 h, the fluorescence from the liver could hardly be observed. A possible reason for this result might be that **Car-BDP-TNM** is mainly eliminated by macrophage cells in liver and spleen.[32]

Potential in vivo toxicity is a great concern in the development of PDT reagents. Besides measuring body weights of mice in each cohort (Figure S19), we also collected the H&E stained images of major organs (heart, liver, spleen, lung, and kidney) from healthy mice and those treated with **Car-BDP-TNM** as well as irradiation (Figure S20). Neither noticeable organ damage nor inflammation lesions can be observed in the irradiated, treated group, by comparison with the healthy mice, which suggests that no obvious heart, liver, spleen, lung, or kidney dysfunctions of the mice were induced by the PDT process using **Car-BDP-TNM**. Further, the serum analysis experiment has been performed according to the reported protocol.[33,34] As shown in Table S2, we did not observe abnormal results from this serum analysis, which suggests that no observable inflammation was induced. In addition, we have also collected excrement from the mice 96 h after the nanoparticle i.v. injection. Such excrement was dissolved in water and then extracted using dichloromethane. The fluorescence spectra of the extractions were subsequently tested. Compared to the PBS-injected control group, we detected the fluorescence of **Car-BDP** in excrement in the nanoparticle treated group (Figure S29), suggesting that **Car-BDP-TNM** was cleared from the body.[35] All these results demonstrate that the as-designed **Car-BDP-TNM** possesses high biosafety and is highly biocompatible.

Moreover, we evaluated the stability and blood circulation of nanoparticles. Since we found that without polymer coating, the fluorescence of the hydrophobic **Car-BDP** molecule was sensitive to water molecules and was found to be gradually quenched as the amount of water increased, here we utilized this point as an approach and first used 10% FBS serum containing cell culture medium to simulate in vivo conditions. As a result, the fluorescence of **Car-BDP-TNM** remains over 96 h (Figure S28), which suggests that **Car-BDP-TNM** is stable under this condition. Moreover, we also conducted the circulation time measurement of **Car-BDP-TNM** in vivo (Figure S30). From the circulation time result, the fluorescence of **Car-BDP-TNM** was able to be detected for more than 90 h, which also suggests **Car-BDP-TNM** has long in vivo stability and blood circulation.[15−17]

CONCLUSION

We have developed a new photosensitizer, a carbazole substituted BODIPY (**Car-BDP**), which shows remarkably intense absorption and high singlet oxygen quantum yield in the NIR region. PLA−PEG-FA coated **Car-BDP** can form stable, small, biocompatible, organic nanoparticles (**Car-BDP-TNM**) that are biocompatible and capable of targeting tumor with specificity. Rather than using typically used laser light, with the a cost-effective ultralow power lamp light, **Car-BDP-TNM** has demonstrated exceptionally potent tumor volume inhibition efficiency (~80%) in deep tissue level in vivo. This cost-effective light source solution would be particularly important in developing countries where medical supplies are lacking. In addition, the fluorescence of **Car-BDP-TNM** can be used to noninvasively guide PDT and monitor the results. Thus, our two-in-one NIR PDT/imaging biodegradable organic nanoparticles are promising therapeutic and diagnostic candidates for cancer treatment. The photosensitizer may also pave the way for their uses in treating deep-tissue cancer, such as brain cancer or the peritoneal metastasis of ovarian cancer, especially in situations not accessible to regular cancer treatment.

ASSOCIATED CONTENT

Supporting Information

The Supporting Information is available free of charge on the ACS Publications website at DOI: 10.1021/jacs.6b05390.

Experimental section; supporting schemes, figures, and tables (PDF)

AUTHOR INFORMATION

Corresponding Author

*Gang.Han@umassmed.edu

Author Contributions

All authors have given approval to the final version of the manuscript.

Notes

The authors declare no competing financial interest.

ACKNOWLEDGMENTS

This research was supported by the China Scholarship Council (CSC) to L.H. This research was supported by the National Institutes of Health R01MH103133 and the Human Frontier Science RGY-0090/2014.

REFERENCES

(1) Dolmans, D. E. J. G. J.; Fukumura, D.; Jain, R. K. *Nat. Rev. Cancer* **2003**, *3*, 380.

(2) Lovell, J. F.; Liu, T. W. B.; Chen, J.; Zheng, G. *Chem. Rev.* **2010**, *110*, 2839.

(3) Celli, J. P.; Spring, B. Q.; Rizvi, I.; Evans, C. L.; Samkoe, K. S.; Verma, S.; Pogue, B. W.; Hasan, T. *Chem. Rev.* **2010**, *110*, 2795.

(4) Lucky, S. S.; Soo, K. C.; Zhang, Y. *Chem. Rev.* **2015**, *115*, 1990.

(5) Chatterjee, D. K.; Fong, L. S.; Zhang, Y. *Adv. Drug Delivery Rev.* **2008**, *60*, 1627.

(6) Voon, S. H.; Kiew, L. V.; Lee, H. B.; Lim, S. H.; Noordin, M. I.; Kamkaew, A.; Burgess, K.; Chung, L. Y. *Small* **2014**, *10*, 4993.

(7) Mitsunaga, M.; Ogawa, M.; Kosaka, N.; Rosenblum, L. T.; Choyke, P. L.; Kobayashi, H. *Nat. Med.* **2011**, *17*, 1685.

(8) Hu, J.; Tang, Y. A.; Elmenoufy, A. H.; Xu, H. B.; Cheng, Z.; Yang, X. L. *Small* **2015**, *11*, 5860.

(9) Wang, C.; Tao, H. Q.; Cheng, L.; Liu, Z. *Biomaterials* **2011**, *32*, 6145.

(10) Idris, N. M.; Gnanasammandhan, M. K.; Zhang, J.; Ho, P. C.; Mahendran, R.; Zhang, Y. *Nat. Med.* **2012**, *18*, 1580.

(11) Punjabi, A.; Wu, X.; Tokatli-Apollon, A.; El-Rifai, M.; Lee, H.; Zhang, Y. W.; Wang, C.; Liu, Z.; Chan, E. M.; Duan, C. Y.; Han, G. *ACS Nano* **2014**, *8*, 10621.

DOI: 10.1021/jacs.6b05390
J. Am. Chem. Soc. 2016, 138, 14586−14591

(12) Gnach, A.; Lipinski, T.; Bednarkiewicz, A.; Rybka, J.; Capobianco, J. A. *Chem. Soc. Rev.* **2015**, *44*, 1561.
(13) Sun, Y.; Feng, W.; Yang, P. Y.; Huang, C. H.; Li, F. Y. *Chem. Soc. Rev.* **2015**, *44*, 1509.
(14) Byrne, A. T.; O'Connor, A. E.; Hall, M.; Murtagh, J.; O'Neill, K.; Curran, K. M.; Mongrain, K.; Rousseau, J. A.; Lecomte, R.; McGee, S.; Callanan, J. J.; O'Shea, D. F.; Gallagher, W. M. *Br. J. Cancer* **2009**, *101*, 1565.
(15) Tian, J. W.; Ding, L.; Xu, H. J.; Shen, Z.; Ju, H. X.; Jia, L.; Bao, L.; Yu, J. S. *J. Am. Chem. Soc.* **2013**, *135*, 18850.
(16) Tian, J. W.; Ding, L.; Ju, H. X.; Yang, Y. C.; Li, X. L.; Shen, Z.; Zhu, Z.; Yu, J. S.; Yang, C. J. *Angew. Chem., Int. Ed.* **2014**, *53*, 9544.
(17) Tian, J. W.; Zhou, J. F.; Shen, Z.; Ding, L.; Yu, J. S.; Ju, H. X. *Chem. Sci.* **2015**, *6*, 5969.
(18) Loudet, A.; Burgess, K. *Chem. Rev.* **2007**, *107*, 4891.
(19) Ulrich, G.; Ziessel, R.; Harriman, A. *Angew. Chem., Int. Ed.* **2008**, *47*, 1184.
(20) Lim, S. H.; Thivierge, C.; Nowak-Sliwinska, P.; Han, J. Y.; van den Bergh, H.; Wagnieres, G.; Burgess, K.; Lee, H. B. *J. Med. Chem.* **2010**, *53*, 2865.
(21) Kamkaew, A.; Burgess, K. *J. Med. Chem.* **2013**, *56*, 7608.
(22) Lu, H.; Mack, J.; Yang, Y. C.; Shen, Z. *Chem. Soc. Rev.* **2014**, *43*, 4778.
(23) Kue, C. S.; Kamkaew, A.; Lee, H. B.; Chung, L. Y.; Kiew, L. V.; Burgess, K. *Mol. Pharmaceutics* **2015**, *12*, 212.
(24) Zhao, J. Z.; Huang, L.; Cui, X. N.; Li, S. J.; Wu, H. J. *J. Mater. Chem. B* **2015**, *3*, 9194.
(25) Zhao, J. Z.; Xu, K. J.; Yang, W. B.; Wang, Z. J.; Zhong, F. F. *Chem. Soc. Rev.* **2015**, *44*, 8904.
(26) He, H.; Lo, P. C.; Yeung, S. L.; Fong, W. P.; Ng, D. K. P. *J. Med. Chem.* **2011**, *54*, 3097.
(27) Ke, M. R.; Yeung, S. L.; Ng, D. K. P.; Fong, W. P.; Lo, P. C. *J. Med. Chem.* **2013**, *56*, 8475.
(28) Cakmak, Y.; Kolemen, S.; Duman, S.; Dede, Y.; Dolen, Y.; Kilic, B.; Kostereli, Z.; Yildirim, L. T.; Dogan, A. L.; Guc, D.; Akkaya, E. U. *Angew. Chem., Int. Ed.* **2011**, *50*, 11937.
(29) Majumdar, P.; Yuan, X. L.; Li, S. F.; Le Guennic, B.; Ma, J.; Zhang, C. S.; Jacquemin, D.; Zhao, J. Z. *J. Mater. Chem. B* **2014**, *2*, 2838.
(30) Kamkaew, A.; Lim, S. H.; Lee, H. B.; Kiew, L. V.; Chung, L. Y.; Burgess, K. *Chem. Soc. Rev.* **2013**, *42*, 77.
(31) Adarsh, N.; Avirah, R. R.; Ramaiah, D. *Org. Lett.* **2010**, *12*, 5720.
(32) Zhang, J. F.; Liang, Y. C.; Lin, X. D.; Zhu, X. Y.; Yan, L.; Li, S. L.; Yang, X.; Zhu, G. Y.; Rogach, A. L.; Yu, P. K. N.; Shi, P.; Tu, L. C.; Chang, C. C.; Zhang, X. H.; Chen, X. F.; Zhang, W. J.; Lee, C. S. *ACS Nano* **2015**, *9*, 9741.
(33) Song, G.; Liang, C.; Yi, X.; Zhao, Q.; Cheng, L.; Yang, K.; Liu, Z. *Adv. Mater.* **2016**, *28*, 2716.
(34) Song, G.; Hao, J.; Liang, C.; Liu, T.; Gao, M.; Cheng, L.; Hu, J.; Liu, Z. *Angew. Chem., Int. Ed.* **2016**, *55*, 2122.
(35) Ishida, T.; Harashima, H.; Kiwada, H. *Biosci. Rep.* **2002**, *22*, 197.

DOI: 10.1021/jacs.6b05390
J. Am. Chem. Soc. 2016, 138, 14586−14591